

Point Jacobi-type preconditioning and parameter tuning for Calderon-preconditioned Burton–Miller method in transmission problems

Keigo Tomoyasu^a, Hiroshi Isakari^{a,*}

^a*Faculty of Science and Technology, Keio University, 3-14-1, Hiyoshi, Kohoku-ku, Yokohama, Kanagawa, 223-8522, Japan*

Abstract

It was recently demonstrated that the boundary element method based on the Burton–Miller formulation (BM-BEM), widely used for solving exterior problems, can be adapted to solve transmission problems efficiently. This approach utilises Calderon’s identities to improve the spectral properties of the underlying integral operator. Consequently, most eigenvalues of the squared BEM coefficient matrix, i.e. the collocation-discretised version of the operator, cluster at a few points in the complex plane. When these clustering points are closely packed, the resulting linear system is well-conditioned and can be solved efficiently using the generalised minimal residual method with only a few iterations. However, when multiple materials with significantly different material constants are involved, some eigenvalues become separated, deteriorating the conditioning. To address this, we propose an enhanced Calderon-preconditioned BM-BEM with two strategies. First, we apply a preconditioning scheme inspired by the point Jacobi method. Second, we tune the Burton–Miller parameters to minimise the condition number of the coefficient matrix. Both strategies leverage a newly derived analytical expression for the eigenvalue clustering points of the relevant operator. Numerical experiments demonstrate that the proposed method, combining both strategies, is particularly effective for solving scattering problems involving composite penetrable materials with high contrast in material properties.

Keywords: Helmholtz’ equation, boundary element method (BEM), the Burton–Miller method, transmission problem, Calderon’s preconditioning

1. Introduction

The boundary element method (BEM) is a numerical method that replaces the boundary value problem (BVP) of partial differential equations (PDEs) with boundary integral equations (BIEs). Unlike standard methods such as the finite element method (FEM) and finite-difference time-domain (FDTD) method, BEM solves BVP by discretising only the boundary of target objects. This feature makes BEM particularly suitable for wave scattering problems involving infinite domains, which are commonly encountered in acoustics, elasticity, and electromagnetics. Among such scattering problems, the so-called *transmission problem*, a mathematical model for wave scattering by penetrable objects, is of great engineering interest due to its wide range of potential applications [1, 2].

So far, various boundary integral formulations for the transmission problem have been proposed, and some of them have been widely used in the BEM community. Among them, PMCHWT (Poggio–Miller–Chang–Harrington–Wu–Tsai) formulation [3], Müller formulation [4] and the single boundary integral equation (SBIE) [5, 6] are especially well recognised as solvers that are free from real-valued fictitious eigenvalues. PMCHWT formulation, one of the most frequently used, can naturally be combined with *Calderon’s preconditioning* [7, 8]. This formulation can thus accelerate the convergence of iterative linear solvers for algebraic

*Corresponding author

Email address: isakari@sd.keio.ac.jp (Hiroshi Isakari)

equations stemming from the BIE. Niino and Nishimura [9] also found that the underlying (discretised version of) integral operator itself can have the role of (the inverse of) preconditioner by appropriately arranging the layer potentials, realising fast convergence for the generalised minimal residual method (GMRES) [10] without explicitly multiplying the preconditioner when the integral equation is discretised by the collocation. The method can easily be extended to the Galerkin BEM with only a few modifications with a cheap preconditioner. The Müller formulation provides an integral equation of the Fredholm second type, thus providing a fast convergence for iterative solvers without any preconditioning. Both methods, however, may have complex-valued fictitious eigenvalues with a tiny imaginary part in its absolute, deteriorating the accuracy even at the real-valued incident frequency that is close to the complex-valued fictitious eigenvalue [11]. On the other hand, the integral operator for SBIE does not involve fictitious eigenvalues around the real axis, thus achieving high efficiency and accuracy. The SBIE requires some special modifications in dealing with multiple materials, though [12]. The multi-trace boundary integral formulation [13] would also be an attractive choice, offering a straightforward extension to the multi-material problem. The formulation, however, requires multiple unknown densities on a single boundary element [13].

The Burton–Miller method [14] has the same distribution for the fictitious eigenvalues with the SBIE and is straightforwardly applicable to multi-material scattering. Iterative solvers for solving (the discretised version of) the boundary integral equations of Burton–Miller type (BM-BIE) can, however, be slow to convergent, especially in the case of transmission problems. Matsumoto et al [15] have recently proposed a Calderon preconditioning for the BM-BIE, in which they designed a well-conditioned integral operator in the sense that its square does not involve any hypersingular operator. Also, the eigenvalues of the square can only accumulate at several points in the complex plane. Especially for the transmission problems with a single material, there exists only one eigenvalue clustering point, reducing the iterative number for GMRES. This formulation can also be applied to multi-material problems. The key idea for accelerating multi-material cases is to use additional Burton–Miller equations not only for unbounded domains but also for some bounded domains. It has already been verified that the Calderon-preconditioned BM-BIE thus constructed achieves the faster convergence by GMRES than the conventional BM-BIE in many cases. Nevertheless, when involving multiple materials with high contrasts in their material constants, such as permittivities and densities, the accumulation points can considerably separate with each other, and thus the GMRES convergence can become slow even with the preconditioning.

Since it is crucial to provide an efficient solver for scattering problems involving composite structures with high-contrast material parameters, especially in complex situations where wave scattering is difficult to control, we present an improved version of the BM-BEM in this paper. We begin by revisiting the BIE formulation in [15], showing that the eigenvalue accumulation can be analytically characterised in general settings. This insight allows us to construct a simple preconditioner, similar to the point Jacobi method, which collapses the clustered eigenvalues into a single point in the complex plane. We also identify both the optimal BM parameters and the interior subdomains to which the BM equations are applied, thereby achieving optimal conditioning of the resulting algebraic system. We demonstrate that the combination of these strategies yields the best overall performance. While the original study [15] demonstrated the efficiency of the approach only in two dimensions, we extend the analysis to three-dimensional problems, further confirming the versatility of both the original and improved Calderon-preconditioned BM-BEM.

The remainder of the paper is organised as follows. In Section 2, we review the BVP of interest and the associated BIEs combined with the Calderon preconditioning introduced in the previous study [15]. We then present an analytical expression for the eigenvalue accumulation of the square of the relevant integral operator. Based on this result, Section 3 introduces an efficient point Jacobi-like preconditioning strategy, together with parameter optimisation techniques, to accelerate the BEM solver. Numerical examples in Section 4 demonstrate the performance of the proposed method, showing that it is highly efficient across a range of cases. Finally, Section 5 concludes the paper and discusses potential directions for future work.

2. Formulation of BM-BIE with Calderon’s preconditioning

In this section, we examine in depth the recently proposed BEM incorporating Calderon’s preconditioning [15] as a preliminary step toward the presentation of the proposed point Jacobi-like preconditioning

and parameter tuning. After stating the boundary value problem of interest in Section 2.1, we outline the BIE formulated in the previous study in Section 2.2. We then present an analytical investigation of the eigenvalue accumulation points of the underlying integral operator in Section 2.3. This theoretical insight will serve as a foundation for the developments in the subsequent sections.

2.1. Statement of the boundary value problem

Let us consider that \mathbb{R}^3 is partitioned into M subdomains as $\bigcup_{i=1}^M \overline{\Omega_i}$ with a sole unbounded domain Ω_1 . Given an incident field $u^{\text{in}} : \Omega_1 \rightarrow \mathbb{C}$ satisfying the three-dimensional Helmholtz equation of wavenumber k_1 , the total field $u : \mathbb{R}^3 \rightarrow \mathbb{C}$ solves the following boundary value problem:

$$\nabla^2 u(\mathbf{x}) + k_i^2 u(\mathbf{x}) = 0 \quad \mathbf{x} \in \Omega_i, \quad (1)$$

$$\lim_{\eta \downarrow 0} u(\mathbf{x} + \eta \mathbf{n}) = \lim_{\eta \downarrow 0} u(\mathbf{x} - \eta \mathbf{n}) \quad \mathbf{x} \in \Gamma, \quad (2)$$

$$\lim_{\eta \downarrow 0} w(\mathbf{x} + \eta \mathbf{n}) = \lim_{\eta \downarrow 0} w(\mathbf{x} - \eta \mathbf{n}) \quad \mathbf{x} \in \Gamma, \quad (3)$$

$$\lim_{|\mathbf{x}| \rightarrow \infty} |\mathbf{x}| \left(\frac{\partial}{\partial |\mathbf{x}|} - ik_1 \right) (u(\mathbf{x}) - u^{\text{in}}(\mathbf{x})) = 0, \quad (4)$$

where $k_i > 0$ denotes the wavenumber of waves propagating in Ω_i , defined by $k_i := \omega \sqrt{\varepsilon_i}$. Here, $\omega > 0$ is the angular frequency of the incident wave, and $\varepsilon_i > 0$ (for $i = 1, \dots, M$) is the material constant associated with Ω_i . The boundary conditions given in (2) and (3) on the boundary $\Gamma := \bigcup_{i=1}^M \partial\Omega_i$ impose jump relations on the total field and its flux. The flux here is defined as $w := \frac{1}{\varepsilon_i} \mathbf{n} \cdot \nabla u$, where \mathbf{n} is the unit normal vector on Γ . On $\partial\Omega_1$, \mathbf{n} is oriented outward from Ω_1 . On the remaining parts of the boundary, the direction of \mathbf{n} is chosen arbitrarily. We also define the boundary $\Gamma_{ij} := \partial\Omega_i \cap \partial\Omega_j$, on which \mathbf{n} is taken to point from Ω_i toward Ω_j . Note that, under this convention, Γ_{i1} (for $i = 2, \dots, M$) does not exist. To ensure the uniqueness of the solution to the boundary value problem, the radiation condition (4) is also imposed at infinity, where i denotes the imaginary unit.

2.2. Calderon-preconditioned BM-BEM

To introduce the recently proposed Calderon-preconditioned BM-BIE, developed by Matsumoto et al [15], for a general setting, we first set up the necessary notation. Let \mathcal{T}_i be the set of indices j such that Ω_i and Ω_j share a common boundary, and let \mathcal{T}_i^+ (resp. \mathcal{T}_i^-) be a subset of \mathcal{T}_i , where the normal vector on $\partial\Omega_i \cap \partial\Omega_j$ is directed from Ω_i (resp. from Ω_j for each $j \in \mathcal{T}_i^-$). We also denote the traces of u and w on Γ_{ij} by u_{ij} and w_{ij} , respectively. With these notations, the boundary value problem (1)–(4) is transformed into the following BIEs on $\mathbf{x} \in \Gamma_{ij}$:

$$\begin{aligned} & -\frac{\alpha_1}{2} u_{ij}(\mathbf{x}) + \sum_{p \in \mathcal{T}_j^-} \alpha_1 [\mathcal{D}_{\Gamma_{pj}}^j u_{pj}](\mathbf{x}) - \sum_{p \in \mathcal{T}_j^+} \alpha_1 [\mathcal{D}_{\Gamma_{jp}}^j u_{jp}](\mathbf{x}) \\ & - \sum_{p \in \mathcal{T}_j^-} \alpha_1 \varepsilon_j [\mathcal{S}_{\Gamma_{pj}}^j w_{pj}](\mathbf{x}) + \sum_{p \in \mathcal{T}_j^+} \alpha_1 \varepsilon_j [\mathcal{S}_{\Gamma_{jp}}^j w_{jp}](\mathbf{x}) = 0, \end{aligned} \quad (5)$$

$$\begin{aligned} & \frac{1}{2} u_{ij}(\mathbf{x}) + \sum_{p \in \mathcal{T}_i^+} [(\mathcal{D}_{\Gamma_{ip}}^i + \alpha_i \mathcal{N}_{\Gamma_{ip}}^i) u_{ip}](\mathbf{x}) - \sum_{p \in \mathcal{T}_i^-} [(\mathcal{D}_{\Gamma_{pi}}^i + \alpha_i \mathcal{N}_{\Gamma_{pi}}^i) u_{pi}](\mathbf{x}) \\ & + \frac{\alpha_i \varepsilon_i}{2} w_{ij}(\mathbf{x}) - \sum_{p \in \mathcal{T}_i^+} \varepsilon_i [(\mathcal{S}_{\Gamma_{ip}}^i + \alpha_i (\mathcal{D}_{\Gamma_{ip}}^i)^*) w_{ip}](\mathbf{x}) + \sum_{p \in \mathcal{T}_i^-} \varepsilon_i [(\mathcal{S}_{\Gamma_{pi}}^i + \alpha_i (\mathcal{D}_{\Gamma_{pi}}^i)^*) w_{pi}](\mathbf{x}) \\ & = \delta_{i1} (u_{1j}^{\text{in}}(\mathbf{x}) + \alpha_1 \varepsilon_1 w_{1j}^{\text{in}}(\mathbf{x})), \end{aligned} \quad (6)$$

where δ_{ij} is the Kronecker delta, and α_i is the coupling coefficient of the Burton–Miller method. In this study, $\alpha_1 = -i/k_1$ is used to keep the complex-valued fictitious eigenvalue away from the real axis [16]. The

settings of α_i for $i \neq 1$ shall be discussed later. The integral operators in (5) and (6) are defined as

$$[\mathcal{S}_\Gamma^i w](\mathbf{x}) := \int_\Gamma G_i(\mathbf{x} - \mathbf{y}) w(\mathbf{y}) d\Gamma(\mathbf{y}), \quad (7)$$

$$[\mathcal{D}_\Gamma^i u](\mathbf{x}) := \int_\Gamma \frac{\partial G_i(\mathbf{x} - \mathbf{y})}{\partial \mathbf{n}(\mathbf{y})} u(\mathbf{y}) d\Gamma(\mathbf{y}), \quad (8)$$

$$[(\mathcal{D}_\Gamma^i)^* w](\mathbf{x}) := \int_\Gamma \frac{\partial G_i(\mathbf{x} - \mathbf{y})}{\partial \mathbf{n}(\mathbf{x})} w(\mathbf{y}) d\Gamma(\mathbf{y}), \quad (9)$$

$$[\mathcal{N}_\Gamma^i u](\mathbf{x}) := \text{p.f.} \int_\Gamma \frac{\partial^2 G_i(\mathbf{x} - \mathbf{y})}{\partial \mathbf{n}(\mathbf{x}) \partial \mathbf{n}(\mathbf{y})} u(\mathbf{y}) d\Gamma(\mathbf{y}), \quad (10)$$

where G_i in (7)–(10) is the following fundamental solution of the three-dimensional Helmholtz equation:

$$G_i(\mathbf{x}) := \frac{e^{ik_i|\mathbf{x} - \mathbf{y}|}}{4\pi|\mathbf{x} - \mathbf{y}|} \quad (11)$$

that satisfies the outgoing radiation condition, and “p.f.” in (10) refers to the finite part of the diverging integral.

Let us now consider all index pairs (i, j) such that $\Gamma_{ij} \neq \emptyset$. These pairs are collected into an ordered set, denoted by \mathcal{B} . The BIE system is then constructed by listing the equations corresponding to (5) for all $(i, j) \in \mathcal{B}$ in order, followed by those corresponding to (6) in the same order. Based on \mathcal{B} , we also define $u_{\mathcal{B}}$ and $w_{\mathcal{B}}$ as ordered lists of functions that collect all u_{ij} s and w_{ij} s, respectively, according to the order in \mathcal{B} . With these settings, we obtain the following system of BIEs:

$$\mathcal{A} \begin{pmatrix} u_{\mathcal{B}} \\ w_{\mathcal{B}} \end{pmatrix} = \text{right-hand side}, \quad (12)$$

where the integral operator \mathcal{A} represents a block operator acting on the ordered pair $(u_{\mathcal{B}}, w_{\mathcal{B}})^t$. It is constructed by stacking the boundary integral operators corresponding to (5) and (6) for each $(i, j) \in \mathcal{B}$, in the order determined by \mathcal{B} . Accordingly, \mathcal{A} consists of $2N_{\mathcal{B}} \times 2N_{\mathcal{B}}$ blocks, with $N_{\mathcal{B}} := |\mathcal{B}|$. To clarify the notation and the procedure described above for constructing BIEs, we provide an illustrative example for a specific geometry in Appendix A.

The system of BIEs (12) differs from the standard formulation in two ways. First, the “upper-half” corresponding to (5) is scaled by $-\alpha_1$. Second, all of the “lower-half” corresponding to (6) are of the BM type. Just to avoid the fictitious eigenvalue problem, it is sufficient to apply the BM formulation only to the equation corresponding to the unbounded domain Ω_1 , i.e., the coupling coefficient α_i can be set to zero for all $i \neq 1$. Nonetheless, Matsumoto et al [15] proposed setting nonzero values for all α_i s red in (6). This, along with the first manipulation, improves the spectral properties of \mathcal{A} , as shall be discussed in the next subsection.

In the formulation of the BIE on Γ_{ij} , the trace from the domain Ω_j is handled by the standard integral equation (5), while that from Ω_i is handled by the BM equation (6). As mentioned above, however, in the case of $i \neq 1$, we may arbitrarily choose which trace to treat as the BM type. As shall be discussed later, the spectral properties of the integral operator \mathcal{A} depend significantly on which side of the boundary is treated by the BM equation. In Section 3.2.2, we shall discuss how to appropriately select which integral equation to apply the Burton–Miller formulation to. Note that in our implementation, since we have decided to associate the orientation of the normal with the type of integral equation in a one-to-one correspondence as shown in (5) and (6), the choice of which integral equation to apply the Burton–Miller formulation to can be made by adjusting the direction of the normal.

2.3. Analytical evaluation of accumulated eigenvalues of the integral operator

Let us now consider solving, by the GMRES [10], the system of linear equations obtained by discretising the system of BIEs (12) using the collocation method and accelerating the GMRES convergence. To this

end, it is insightful to investigate the accumulation points of the eigenvalues of the square of the integral operator \mathcal{A} [9]. Through a detailed and rigorous calculation based on the integral equations (5) and (6), and Calderon's formula, we found that \mathcal{A}^2 assumes the following form:

$$\mathcal{A}^2 = \begin{pmatrix} \lambda_1 \mathcal{I} & & & 0 \\ & \ddots & & \\ & & \lambda_{N_{\mathcal{B}}} \mathcal{I} & \\ c_1 \mathcal{I} & & & \lambda_{N_{\mathcal{B}}+1} \mathcal{I} \\ & \ddots & & \\ 0 & & c_{N_{\mathcal{B}}} \mathcal{I} & \lambda_{2N_{\mathcal{B}}} \mathcal{I} \end{pmatrix} + \mathcal{K}, \quad (13)$$

where \mathcal{I} is the identity operator, λ_i and c_i are complex constants, and \mathcal{K} represents an integral operator whose eigenvalues accumulate only at the origin of the complex plane [8, 9]. The eigenvalue accumulation of the squared operator \mathcal{A}^2 is thus characterised by the operator whose upper-triangular blocks are all zero operators. The clustered eigenvalues λ_{i_b} for $i_b = 1, \dots, 2N_{\mathcal{B}}$ are, of course, identical to the coefficients of the identity operators in the diagonal, given by

$$\begin{cases} \lambda_{i_b} = \frac{\alpha_1^2}{4} \left(1 + \frac{\alpha_i}{\alpha_1} \varepsilon_j \right) \\ \lambda_{i_b+N_{\mathcal{B}}} = \frac{\alpha_1^2}{4} \left(\frac{\alpha_i^2}{\alpha_1^2} \varepsilon_i^2 + \frac{\alpha_i}{\alpha_1} \varepsilon_j \right) \end{cases}, \quad (14)$$

for $1 \leq i_b \leq N_{\mathcal{B}}$, where (i, j) is the i_b -th entry of the ordered list \mathcal{B} . The square of the integral operator in (12) thus has at most $2N_{\mathcal{B}}$ accumulated eigenvalues, regardless of the choice of the arbitrary parameters α_i for $i = 2, \dots, M$. From (14), it is now clear why additional BM equations are necessary. When $\alpha_i = 0$, the operator acquires a zero eigenvalue, which can significantly increase the condition number of the BEM coefficient matrix obtained through discretisation.

Matsumoto et al [15] set $\alpha_i = \alpha_1/\varepsilon_i$ based purely on empirical reasoning. By examining our findings in (14), however, one may observe that this setting actually leads to the following relation:

$$\lambda_{i_b} = \lambda_{i_b+N_{\mathcal{B}}} = \frac{\alpha_1^2}{4} \left(1 + \frac{\varepsilon_j}{\varepsilon_i} \right) \quad \text{for } 1 \leq i_b \leq N_{\mathcal{B}}. \quad (15)$$

This setting can therefore reduce the number of accumulation points to $N_{\mathcal{B}}$ from $2N_{\mathcal{B}}$. Most of the eigenvalues of the matrix \mathbf{A}^2 obtained by discretising the operator \mathcal{A}^2 via collocation are then expected to lie near these points, which may lead to faster convergence of GMRES. Note that it is not necessary to explicitly compute the squared matrix to take advantage of the improved conditioning of \mathbf{A}^2 , since GMRES constructs approximate solutions in the Krylov subspace $\text{span}\{\mathbf{x}_0, \mathbf{A}\mathbf{x}_0, \mathbf{A}^2\mathbf{x}_0, \dots\}$, where \mathbf{x}_0 is the initial estimate for the solution of the system of linear equations.

The above α_i setting does, unfortunately, not always accelerate the GMRES convergence. For example, when the target domain consists of multiple materials with significantly different material constants, the eigenvalue accumulation points may be widely separated. In such cases, the condition number of \mathbf{A}^2 can still be large, resulting in poor convergence of GMRES. This motivates us to seek further improvements in the conditioning of the underlying system. In the next section, which presents the main contribution of this paper, we propose novel strategies to further improve the conditioning of the system.

3. Strategies for further improving the BIE conditioning

This section proposes two methods for the Calderon-preconditioned BM-BIE in the preceding section to improve its conditioning, particularly in cases where the contrast in material constants is large in multi-material settings. One method enforces eigenvalue accumulation at a single point by applying a simple preconditioner, while the other adjusts the parameters α_i for $i = 2, \dots, M$ and normal orientations to bring the eigenvalues closer together.

3.1. Point Jacobi-type preconditioning

Since the accumulated eigenvalues (14) for the squared integral operator \mathcal{A}^2 in the BIE system (12) have now been analytically identified, one may use a point Jacobi-like preconditioner \mathcal{M} to adjust the operator, such that all the clustered eigenvalues of $(\mathcal{A}\mathcal{M}^{-1})^2$ are shifted to 1. This can be achieved by defining \mathcal{M} as

$$\mathcal{M} = \text{diag}(\sqrt{\lambda_1}\mathcal{I}, \sqrt{\lambda_2}\mathcal{I}, \dots, \sqrt{\lambda_{2N_{\mathcal{B}}}}\mathcal{I}), \quad (16)$$

where \mathcal{M} has the same block structure as \mathcal{A} . It is thus expected that the collocation-discretised version of the (square of) preconditioned operator $(\mathcal{A}\mathcal{M}^{-1})^2$ is close to the identity matrix, with a considerably small condition number. As a result, we may expect an improvement in the convergence of the iterative solver.

It is worth noting that the preconditioning defined in this way can be both efficiently implemented and applied with little computational overhead. We can explicitly evaluate \mathcal{M}^{-1} and store only the square root of the reciprocal of the estimated eigenvalues in (14), i.e., we only need an array of size equal to the number $2N_{\mathcal{B}}$ of the eigenvalue accumulation points, which hardly increases memory usage. In addition, we do not need to explicitly evaluate the preconditioned matrix $\mathcal{A}\mathcal{M}^{-1}$. Instead, we simply multiply the diagonal matrix \mathcal{M}^{-1} to the Krylov basis before multiplying by \mathcal{A} .

Note, however, that the squared coefficient matrix \mathcal{A}^2 may have eigenvalues that deviate from the estimated locations (14) in the complex plane. If such an eigenvalue lies close to (resp. far from) the origin, multiplying the inverse of preconditioner \mathcal{M}^{-1} with a tiny (resp. huge) diagonal entry may amplify the condition number of the preconditioned matrix $\mathcal{A}\mathcal{M}^{-1}$ and consequently that of its square $(\mathcal{A}\mathcal{M}^{-1})^2$. It is therefore important to construct \mathcal{A} and \mathcal{M} in such a way that \mathcal{M} is close to the identity matrix, which corresponds to having all the eigenvalue accumulation points of \mathcal{A}^2 tightly packed. This may be achieved by appropriately setting the BIEs (5) and (6) with optimised tunable parameters α_i for $i = 2, \dots, M$, which will be addressed in the next subsection.

3.2. Minimising the maximum pairwise ratios of accumulated eigenvalues of \mathcal{A}^2

In this subsection, we formulate the BIE system (12) so as to minimise the maximum ratio between the absolute values of any two accumulated eigenvalues of the operator \mathcal{A}^2 , while keeping the number of accumulated eigenvalues fixed at $N_{\mathcal{B}}$. Specifically, we consider which integral equations should be formulated in the BM form, and how the parameters α_i for $i = 2, \dots, M$ in the BM equations should be chosen. Recall that the former is achieved by appropriately setting the normal direction as discussed at the end of Subsection 2.3. These approaches also improve the effectiveness of the point Jacobi method, as the eigenvalues become tightly clustered and \mathcal{M}^{-1} in (16) becomes close to the identity operator.

3.2.1. Possible α_i choices for $i = 2, \dots, M$

Let us temporarily fix the normal directions and investigate all possible choices of the parameters α_i for $i = 2, \dots, M$ that lead to the eigenvalues of \mathcal{A}^2 to cluster at $N_{\mathcal{B}}$ points. The original setting

$$\gamma_i := \frac{\alpha_i}{\alpha_1} = \frac{1}{\varepsilon_i} \quad (17)$$

in [15] satisfies this requirement. We shall henceforth refer to this setting as P1. Let us now take the i_b -th element (i, j) and the j_b -th element (k, ℓ) from the index set \mathcal{B} , and consider the corresponding BM-BIEs (6) defined on Γ_{ij} and $\Gamma_{k\ell}$. We assume here that α_k is fixed according to P1, under which the relation $\lambda_{j_b} = \lambda_{j_b+N_{\mathcal{B}}}$ holds. With this setting, we may choose γ_i such that $\lambda_{i_b} = \lambda_{j_b} = \lambda_{j_b+N_{\mathcal{B}}}$, yielding

$$\gamma_i = \frac{\varepsilon_{\ell}}{\varepsilon_k \varepsilon_j}. \quad (18)$$

We refer to this setting as P2. It is also possible to set γ_i such that $\lambda_{i_b+N_{\mathcal{B}}} = \lambda_{j_b} = \lambda_{j_b+N_{\mathcal{B}}}$, which gives the following P3:

$$\gamma_i = \frac{-\varepsilon_j + \sqrt{\varepsilon_j^2 + 4\varepsilon_i^2(1 + \varepsilon_{\ell}/\varepsilon_k)}}{2\varepsilon_i^2}. \quad (19)$$

In deriving (19), we reject negative values of γ_i , since having α_i share the sign as α_1 ensures that all fictitious and complex-valued eigenvalues arising from the BM equation have negative imaginary parts.

Recalling that the use of either P1 in (17), P2 in (18), or P3 in (19) for the artificial BM parameter effectively limits the number of accumulation points to N_B , it is sufficient to choose the parameter that minimises the ratio between the absolute values of the accumulated eigenvalues of \mathcal{A}^2 among these options.

In searching for the optimal parameter setting among the candidates (17)–(19) while preserving the number of eigenvalue accumulation points, we must additionally impose the following two constraints:

C1 If multiple subdomains are adjacent to Ω_i , and the outward normal vectors on $\partial\Omega_i$ point towards at least two of these adjacent subdomains, then γ_i must be chosen according to P1 (Fig. 1).

C2 If ε_i appears in γ_k for the BM-BIE on $\Gamma_{k\ell}$ with $\ell \neq i$, then α_i must be fixed according to P1.

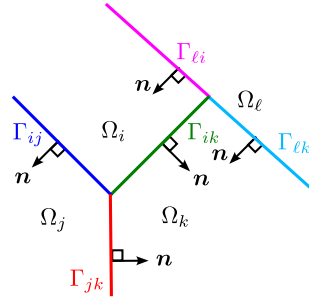


Figure 1: Illustration of condition C1, in which the parameter α_i is fixed using P1. Since the outward normal on $\partial\Omega_i$ points into both Ω_j and Ω_k , the BM equations derived from Ω_i with $\alpha_i = \alpha_1/\varepsilon_i$ are applied on Γ_{ij} and Γ_{ik} . On Γ_{il} , the BIE derived from Ω_i should be of the standard type, as the normal on this boundary points into Ω_i . Instead, the BIE on Γ_{il} derived from Ω_ℓ is of the BM type.

3.2.2. Setting direction of normal vectors

We then discuss an appropriate choice of normal directions, thereby ensuring that the suitable equations are formulated in the BM-type, as discussed in Subsection 2.3, which improves the conditioning of the system of BIEs (12). To see how the normal direction setting influences the eigenvalue distribution of \mathcal{A}^2 , let us consider the case where all the parameters α_i s of P1 are used for a geometry depicted in Figure 2, with material constants $\varepsilon_1 = 1$, $\varepsilon_2 \simeq 1$, and $\varepsilon_3 \ll 1$. In this case, \mathcal{A}^2 has two eigenvalue accumulation points,

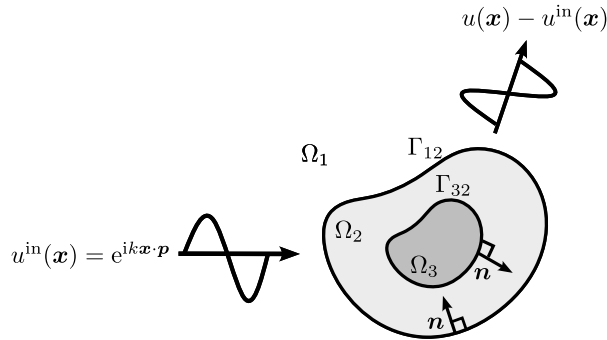


Figure 2: Multiple domains.

given by $\frac{\alpha_1^2(1+\varepsilon_2)}{4}$ and $\frac{\alpha_1^2(1+\varepsilon_2/\varepsilon_3)}{4}$, the ratio of whose absolute values is considerably large. On the other

hand, when the normal vector on $\partial\Omega_2 \cap \partial\Omega_3$ is flipped, i.e. when Γ_{32} is redefined as Γ_{23} , the accumulation points become $\frac{\alpha_1^2(1+\varepsilon_2)}{4}$ and $\frac{\alpha_1^2(1+\varepsilon_3/\varepsilon_2)}{4}$, which are much closer to each other than those in the previous configuration. Note that we cannot flip the normal on $\partial\Omega_1$, since the BIE corresponding to the unbounded domain Ω_1 must be of the BM type to avoid the fictitious eigenvalue problem.

3.2.3. Algorithm to optimise parameters α_i for $i = 2, \dots, M$

By combining the parameter settings described in Subsection 3.2.1 with normal direction flipping as discussed in Subsection 3.2.2, we determine the optimal configuration of the BIE system (12). Specifically, we perform an exhaustive search over all admissible combinations of the parameter settings (17)–(19), subject to C1 and C2, along with all possible normal orientations. For each configuration, we compute the accumulation points of the eigenvalues of \mathcal{A}^2 and evaluate the maximum ratio between the absolute values of any two such accumulation points. The configuration that minimises this maximum ratio is selected as the optimal one, as it yields the best spectral properties and thus improves the conditioning of the system.

4. Numerical examples

This section presents numerical experiments to verify that the proposed parameter tuning and simple preconditioning can accelerate the Calderon-preconditioned BM-BEM proposed in [15]. We first demonstrate in Subsection 4.1 that the conventional Calderon-preconditioned BM-BEM, without the proposed parameter tuning and point Jacobi-like preconditioning, performs well in many cases but may fail to accelerate GMRES convergence in others. We then show in Subsection 4.2 that applying both strategies significantly improves the performance.

In all the following examples, we employ a collocation discretisation with piece-wise constant elements for the BM-BIEs. The singular parts of the boundary integrals are evaluated analytically, while the remaining parts are computed numerically using Gauss–Legendre (GL) quadrature with 16 nodes. Hypersingular integrals are regularised, and the resulting line integrals are evaluated using GL quadrature with 10 nodes. The resulting linear systems are solved using GMRES, with the tolerance set to 10^{-5} .

4.1. Performance evaluation of the conventional Calderon-preconditioned BM-BEM

Let us first examine the accuracy and efficiency of the Calderon-preconditioned BM-BEM using a benchmark problem for which the analytical solution is available. To this end, we consider a multi-material configuration with $M = 3$, as illustrated in Figure 3. A spherical inclusion Ω_3 of radius 0.5 is completely embedded within another spherical object Ω_2 of radius 1.0, and both share the same centre at the origin. The outermost domain, the host matrix Ω_1 , along with the inclusions Ω_2 and Ω_3 , have material constants 1, 2, and 3, respectively. As the incident wave, we use a plane wave propagating in the direction of the x_2 -axis with angular frequency $\omega = 5.0$.

In this configuration, according to our formulation, the unit normal vector on $\partial\Omega_1 \cap \partial\Omega_2$ should be consistently oriented outward from Ω_1 , since the BIE corresponding to the exterior domain Ω_1 must be of BM type. On the other hand, the unit normal on $\partial\Omega_2 \cap \partial\Omega_3$ can, in principle, be arbitrarily oriented, but is here temporarily fixed to point outward from Ω_3 ; that is, we apply the BM-BIE for Ω_3 for the time being. As for the Burton–Miller coefficient α_3 , we temporarily fix it here according to P1, i.e., $\alpha_3 = \alpha_1/\varepsilon_3$, as in (17). This choice is consistent with the original paper [15].

Here, we first check the relative ℓ_2 -error in u at the collocation points on $\Gamma_{12} \cup \Gamma_{32}$, computed against the analytical solution, as well as the number of GMRES iterations required by the Calderon-preconditioned BM-BEM, with respect to the number of collocation points N . For comparison, we also compute the same quantities for the conventional BM-BEM, in which $\alpha_3 = 0$ and the integral operators in the upper (5) and lower (6) halves of the operator \mathcal{A} in (12) are interchanged. The ℓ_2 -error here is defined as

$$\text{Error} := \sqrt{\frac{\sum_{i=1}^N |u_{\text{num}}(\mathbf{x}_i) - u_{\text{ana}}(\mathbf{x}_i)|^2}{\sum_{i=1}^N |u_{\text{ana}}(\mathbf{x}_i)|^2}}, \quad (20)$$

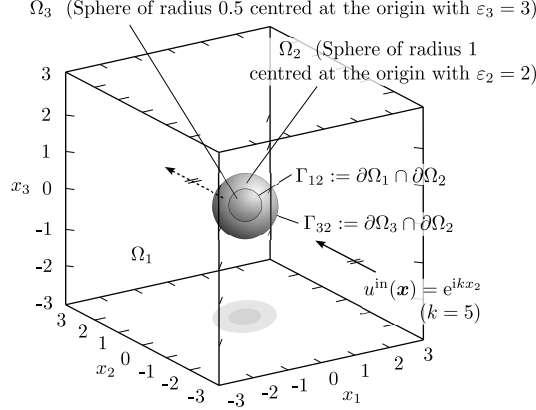


Figure 3: Problem setting for the transmission problem in the multi-material configuration. The normal vectors on the surfaces are directed from Ω_1 and Ω_3 in this setting. The boundaries are thus denoted as Γ_{12} and Γ_{32} .

where u_{num} and u_{ana} are respectively the numerical and analytical solutions, N is the number of the boundary elements, and \mathbf{x}_i is the i -th collocation point, and the analytical solutions u_{ana} in (20) is derived from the following equations:

$$\left\{ \begin{array}{ll} u_{\text{ana}}(\mathbf{x}) = u^{\text{in}}(\mathbf{x}) + \sum_{n=0}^{\infty} \sum_{m=-n}^n a_n^m h_n^{(1)}(k_1|\mathbf{x}|) Y_n^m(\theta, \phi) & \mathbf{x} \in \Omega_1 \\ u_{\text{ana}}(\mathbf{x}) = \sum_{n=0}^{\infty} \sum_{m=-n}^n (b_n^m h_n^{(1)}(k_2|\mathbf{x}|) + c_n^m j_n(k_2|\mathbf{x}|)) Y_n^m(\theta, \phi) & \mathbf{x} \in \Omega_2 \\ u_{\text{ana}}(\mathbf{x}) = \sum_{n=0}^{\infty} \sum_{m=-n}^n d_n^m j_n(k_3|\mathbf{x}|) Y_n^m(\theta, \phi) & \mathbf{x} \in \Omega_3, \end{array} \right. \quad (21)$$

where a_n^m , b_n^m , c_n^m and d_n^m are complex constants determined, exploiting the orthogonality of the spherical harmonics, by the boundary conditions in (2) and (3). Also, j_n and $h_n^{(1)}$ are respectively the n^{th} order spherical Bessel function and Hankel function of 1st kind, and Y_n^m is spherical harmonics defined as

$$Y_n^m(\theta, \phi) = \sqrt{\frac{(n-m)!}{(n+m)!}} P_n^m(\cos \theta) e^{im\phi}, \quad (22)$$

where P_n^m is the associated Legendre polynomial, and θ and ϕ denote the polar and azimuthal angles for \mathbf{x} respectively. In our computation, the infinite sums for n in (21) is truncated by its first 51 terms.

Figure 4 presents the results. The left panel of Figure 4 shows that the accuracy of the preconditioned BM-BIE does not exactly match that of the conventional formulation, since the BM-BIE being solved differs between the two approaches. However, the difference in error is not significant. In the present case, the accuracy is slightly degraded for large N by the proposed formulation, but this is not always the case; depending on the configuration, we have observed that the use of additional BM equations for interior domains can even improve accuracy in some cases [17]. The right panel shows that the Calderon preconditioning substantially reduces the number of GMRES iterations. More importantly, the proposed BM-BEM achieves a nearly constant iteration number regardless of the number of boundary elements N . Appendix B provides further insight into how manipulating the eigenvalue distribution of the operator \mathcal{A}^2 leads to a reduced number of GMRES iterations.

To examine the versatility of the method, we evaluate the number of GMRES iterations under various settings of angular frequency ω and material constants ε_i with the number of boundary elements fixed at $N = 57600$. The left panel of Figure 5 shows the case where the angular frequency ω is swept over the

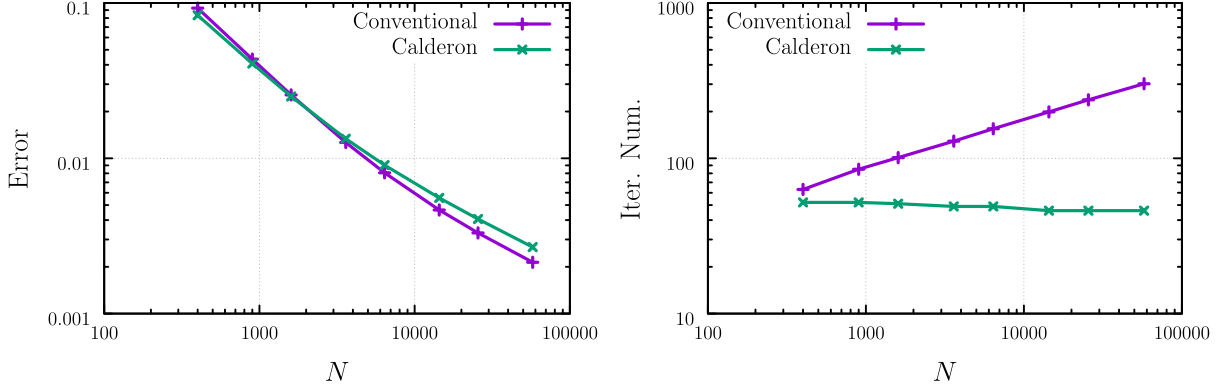


Figure 4: (Left) The relative ℓ_2 -error versus N for wave scattering by concentric spheres. (Right) The number of GMRES iterations.

range $0 < \omega \leq 5$, with the material constants fixed as $\varepsilon_i = i$ for $i = 1, \dots, 3$. The right panel corresponds to the case where ε_3 is swept in the range $0 < \varepsilon_3 \leq 10$, while the other parameters are set as $\varepsilon_1 = 1$ and $\varepsilon_2 = 1/\varepsilon_3$. In this case, the angular frequency is fixed to $\omega = 5.0$. Figure 5 demonstrates that the

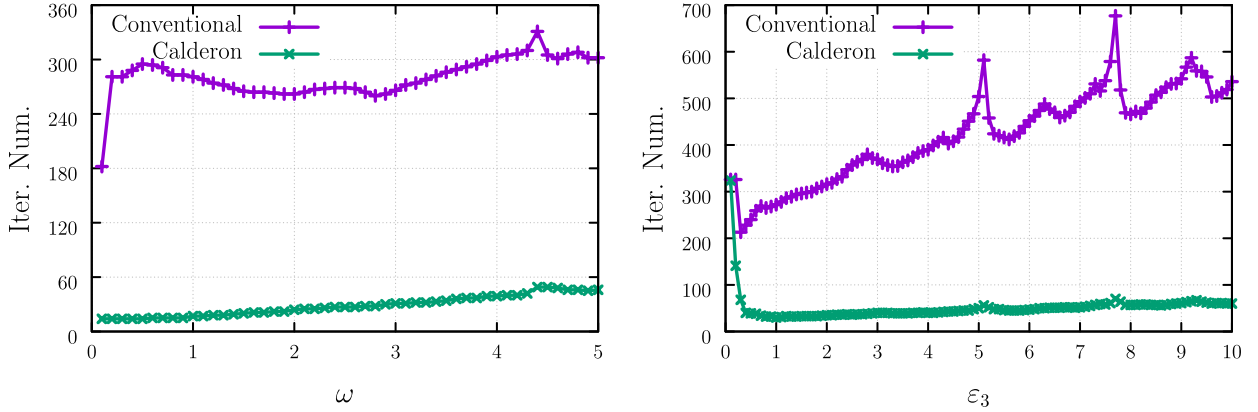


Figure 5: Number of GMRES iterations versus ω (left) and ε_3 (right) for wave scattering by concentric spheres.

Calderon-preconditioned BEM requires fewer GMRES iterations than the conventional formulation for all tested parameter settings. It can, however, be observed that the performance may degrade significantly with a large contrast between ε_2 and ε_3 . In particular, when $\varepsilon_3 \ll 1$ (and correspondingly $\varepsilon_2 \gg 1$), the number of iterations required by the preconditioned system is almost the same as that of the conventional one.

We next examine a case involving geometry with junctions and corners. To this end, we consider the scattering by two cuboids, Ω_2 and Ω_3 , which are in contact along one face, as illustrated in Figure 6. The left panel of Figure 7 shows the number of GMRES iterations as a function of the number of boundary elements, N , using the same parameters as in the previous concentric spheres case; the angular frequency and material constants are fixed at $\omega = 5$, $\varepsilon_1 = 1$, $\varepsilon_2 = 2$, and $\varepsilon_3 = 3$. The centre and right panels correspond to those in Figure 5, which show the dependence of the GMRES iterations on the angular frequency and material constants. For these computations, the number of boundary elements was fixed at $N = 57344$.

We can draw similar conclusions to those in the case of concentric spheres. The Calderon-preconditioned BM-BEM requires an almost constant number of GMRES iterations, regardless of the number of boundary elements, and generally performs better than the conventional method, even when the scatterers being analysed have junctions and corners. However, for material constants with a high contrast, both ends of the

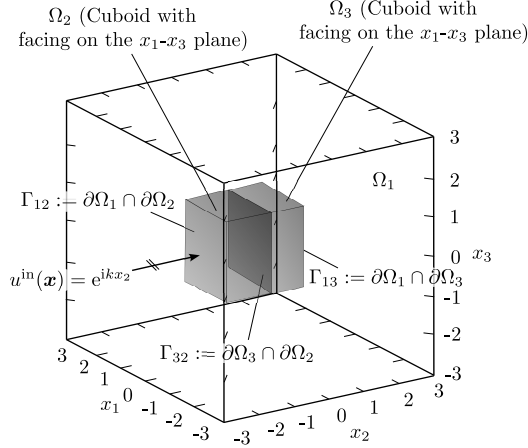


Figure 6: The problem setting for transmission problem with junctions and corners.

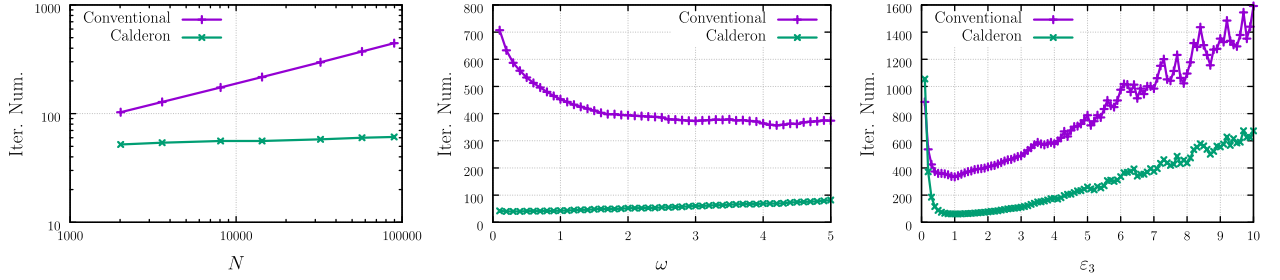


Figure 7: (Left) The number of GMRES iterations vs N for wave scattering by a scatterer in Fig. 6 (centre) the number of iterations vs ω (right) the number of iterations vs ε_2 .

right panel in Figure 7 show an increase in the number of GMRES iterations. In particular, when $\varepsilon_3 \ll 1$, the preconditioned BEM requires even more iterations than the conventional one. We therefore attempt to reduce the number of iterations in such high-contrast cases using the strategies described in Sections 3.

4.2. Effectiveness of the proposed approaches

In this subsection, we verify the effectiveness of the proposed point Jacobi-like preconditioning method and parameter tuning strategy. As an example, we revisit the concentric spheres case under the worst-case parameter settings shown in Figure 5, namely, $\varepsilon_1 = 1.0$, $\varepsilon_2 = 0.1$, and $\varepsilon_3 = 10.0$. In the previous example shown in Figure 5, the number of GMRES iterations was 324. We now apply the proposed point Jacobi-like preconditioner in Subsection 3.1 while keeping the integral equation settings unchanged; that is, we adopt the BM-type BIE formulation for Ω_1 and Ω_3 , and use the parameter $\alpha_3 = \alpha_1/\varepsilon_3$ (referred to as P1) for the latter. The number of GMRES iterations is thereby reduced to 197. As previously noted, since the application of the inverse of the preconditioner matrix incurs negligible computational cost, this significant reduction represents a highly efficient improvement.

While this alone is already promising, further gains can be achieved by tuning the formulation according to Subsection 3.2.3 prior to applying the preconditioner. In the current layered spherical geometry, we may choose the orientation of the interface $\partial\Omega_2 \cap \partial\Omega_3$, i.e. whether it is treated as Γ_{32} or Γ_{23} , that determines which BIE is cast in BM form. Combined with the three parameter patterns (P1, P2, and P3), this gives rise to six possible BIE configurations.

The number of GMRES iterations for each of these configurations, with the point Jacobi-like preconditioning applied, is summarised in Table 1. The table highlights the importance of selecting an appropriate

Table 1: Number of GMRES iterations for different combinations of interface orientation and parameter patterns, with the point Jacobi-like preconditioning applied. The value marked with * shows the untuned configuration discussed in the main text.

Interface	P1	P2	P3
Γ_{32}	197*	181	181
Γ_{23}	219	296	151

BIE system by properly orienting the interface and choosing suitable parameters before applying the preconditioner.

We are thus motivated to combine the parameter tuning with point Jacobi-like preconditioning. Specifically, we first explore the best interface orientation and BM coefficient, aiming to minimise the maximum ratio of the absolute values of the accumulation points of the operator \mathcal{A}^2 . We then solve the linear system using the point Jacobi-like preconditioner defined in (16). With this strategy, we reproduce the results shown in the right panels of Figures 5 and 7, which indicate the number of GMRES iterations required for scattering problems involving concentric spheres and two cuboids, under various settings of the material constants. The results are summarised in Figure 8. In the figure, the results obtained by using the proposed strategy (labelled as “PPM”; Parameter-tuned and Point Jacobi-like Method) are compared those by other approaches. “Calderon” refers to the results presented in the previous subsection, obtained with a fixed interface orientation (as shown in Figures 3 and 6) and the BM parameter fixed to P1. “Param” indicates the use of parameter tuning alone, without any preconditioner, while “Jacobi” applies the point Jacobi preconditioner to the same linear system as “Calderon”. The figures demonstrate that the proposed method,

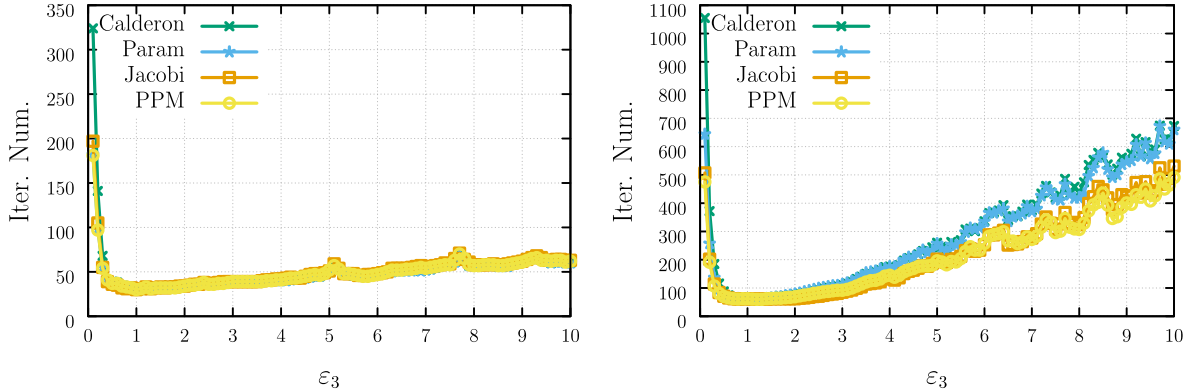


Figure 8: (Left) The number of GMRES iterations vs ε_3 in case of Fig. 3 for wave scattering by an unit sphere (right) the number of iterations vs ε_3 in case of Fig. 6.

which combines both strategies, improves efficiency in almost all cases, particularly in high-contrast material settings.

Figure 8 may give the impression that the proposed method “PPM” performs almost identically to “Jacobi” in many cases, except in the extremely high-contrast settings. Further examination reveals, however, that this is not necessarily the case. To illustrate this, we again consider the scattering by concentric spheres shown in Figure 3, with a different arrangement of material constants: ε_1 and ε_3 are fixed at 1 and 10, respectively, while ε_2 is varied from 0.1 to 10. The number of GMRES iterations required in this setting is presented in Figure 9. In the figure, over a wide range of ε_2 , the performance of “Jacobi” is clearly observed to be inferior to that of “PPM”. This result highlights the critical contribution of the proposed parameter tuning, which serves to enhance the effectiveness of “Jacobi”. One also observes that, for $\varepsilon_2 > 9$, the performance of “Param” deteriorates significantly. These findings suggest that neither “Jacobi” nor “Param”

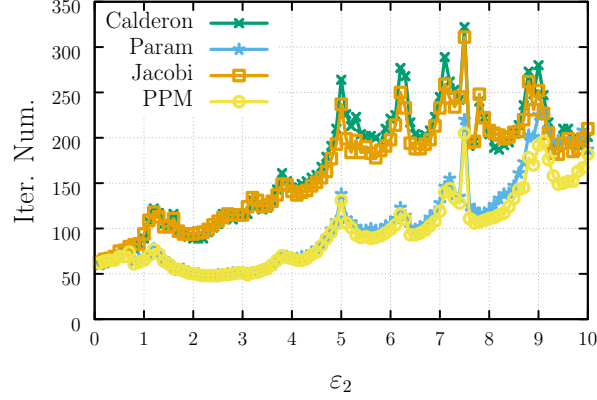


Figure 9: GMRES iteration number with varying material constant of Ω_2 , with $\varepsilon_1 = 1$ and $\varepsilon_3 = 10$ fixed.

alone is sufficient, and that the combined approach employed in “PPM” provides the most robust results.

Given that the eigenvalue accumulation points of the preconditioned squared integral operator $(\mathcal{A}\mathcal{M}^{-1})^2$ are all theoretically forced to be at 1, the poor performance of “Jacobi” observed in Figure 9 may appear counter-intuitive. This discrepancy can be attributed to the fact that the collocation-discretised version of the operator, i.e., the square of preconditioned matrix $(\mathbf{A}\mathbf{M}^{-1})^2$ may deviate from the estimated accumulation point. To demonstrate this, we compute and compare the eigenvalue distributions of the squared matrices associated with both the “Jacobi” and “PPM” methods. The left panel of Figure 10 presents the spectrum for “Jacobi” along with that of “Calderon” method, while the right panel shows the result for “PPM” with “Param”. In these computations, we set $\omega = 1$, $\varepsilon_1 = 1$, $\varepsilon_2 = 4$, $\varepsilon_3 = 10$, and used $N = 2880$ boundary elements. The left panel of the figure shows that many of the eigenvalues for “Calderon” cluster around the

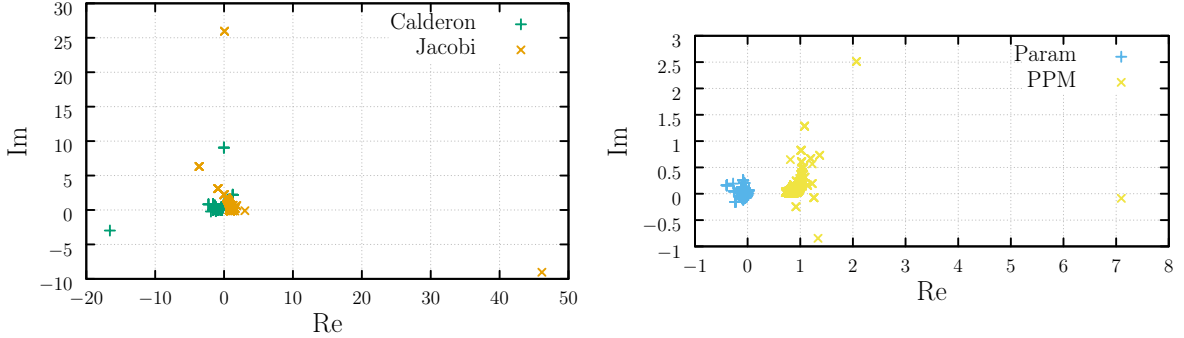


Figure 10: Change in the eigenvalue distribution of \mathbf{A}^2 from that of “Calderon” to “Jacobi” (left) and “Param” to “PPM” (right). Note that the scales of the figures differ considerably.

expected locations, namely -1.25 and -0.35 . These values are derived from equation (15) with $(i, j) = (1, 2)$ and $(3, 2)$, respectively. One can also observe, however, that a few of the eigenvalues lie significantly away from these points. In the eigenvalue distribution for “Jacobi”, also shown in the same panel, such outlying eigenvalues are further amplified in magnitude due to the structure of the preconditioner (16). Recall that the diagonal entries of our preconditioner (its square to be precise) $(\mathbf{M}^{-1})^2$ correspond to the reciprocals of the cluster points. As a result, any deviation from the expected spectral location is magnified in this case. In contrast, this undesired effect can be mitigated in the proposed “PPM” method. Here, we first explore,

via the normal flipping and parameter tuning, a modified BIE formulation whose eigenvalue accumulation points are as close together as possible before applying the preconditioning. The right panel of the figure shows the eigenvalue distribution for this formulation, labeled as “Param”. The associated accumulation points are -1.25 and approximately -1.0698 , the latter obtained from the first equation in (14) with α_i defined in (19), using the tuple $(i, j, k, l) = (2, 3, 1, 2)$. With this design, the preconditioner also becomes closer to the identity matrix and does not scatter the outlier eigenvalues as strongly. Consequently, the eigenvalues in “PPM” tend to remain bounded in magnitude and well-behaved.

As the final numerical example, we examine the versatility of the proposed method in handling scattering from geometrically complex structures. To this end, we consider a composite scatterer composed of four stacked boxes, as shown in Figure 11. Each box, as well as the host matrix, is characterised by specific

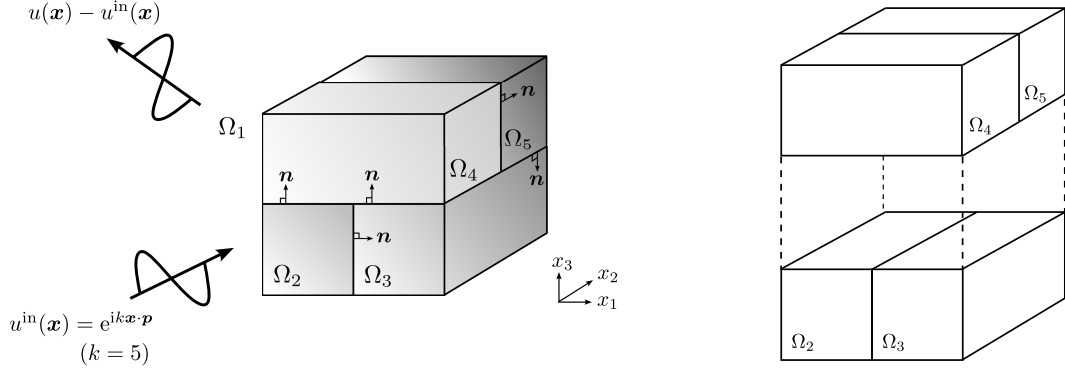


Figure 11: Illustrative sketch of scattering by a composite scatterer consisting of four boxes (left), and its schematic diagram (right). The two lower boxes are aligned along the x_2 -axis, while the two upper boxes are aligned along the x_1 -axis.

material constants. Among these, some are fixed as $\varepsilon_1 = 1$, $\varepsilon_2 = 2$, and $\varepsilon_5 = 3$, while ε_3 and ε_4 vary: ε_3 ranges within $0 < \varepsilon_3 \leq 10$, and ε_4 is set as $\varepsilon_4 = 1/\varepsilon_3$. In the computation, the surfaces of the boxes are discretised into $N = 82944$ triangular boundary elements.

Since the structure is now considerably complex, many possibilities exist to construct the system of BIEs (12). To specify a particular system, we use the ordered set \mathcal{B} of interface pairs, as defined in Subsection 2.2. When the normal vectors on all interfaces are set as shown in Figure 11, this set is given by

$$\mathcal{B} = \{(1, 2), (1, 3), (1, 4), (1, 5), (2, 3), (2, 4), (3, 4), (4, 5), (5, 2), (5, 3)\}. \quad (23)$$

Following the formulation in Subsection 2.2, we assign a BIE to each interface Γ_{ij} with $(i, j) \in \mathcal{B}$ as follows:

- On the side of Ω_j , the standard formulation in (5) is used.
- On the side of Ω_i , the BM-type formulation in (6) is employed.

The BM coefficient α_i used on Γ_{ij} is thus set for the integral equation derived from Ω_i . In particular, for those interfaces that do not involve the exterior domain Ω_1 , we allow multiple choices for α_i , corresponding to P1, P2, or P3. To simplify the notation, we introduce $\Gamma_{ij}(\text{P}^k)$ to indicate that:

- the interface is oriented from Ω_i to Ω_j ,
- the BM-type BIE is applied to Ω_i with parameter choice P^k (e.g., $\alpha_i = \alpha_1/\varepsilon_i$ for $k = 1$),
- and the standard BIE is applied to Ω_j .

With this convention, the entire system of BIEs is fully characterised by the set of such interface notations. For instance, if all interfaces are oriented as shown in the figure, and all BM coefficients are set using P1, the BIE system can be denoted as:

$$\Gamma_{23}(\text{P}^1), \quad \Gamma_{24}(\text{P}^1), \quad \Gamma_{34}(\text{P}^1), \quad \Gamma_{45}(\text{P}^1), \quad \Gamma_{52}(\text{P}^1), \quad \Gamma_{53}(\text{P}^1). \quad (24)$$

Here, the interfaces Γ_{1j} for all j are omitted, as the corresponding BIEs have already been fixed as the preceding discussion. Note that for the parameter α_i on Γ_{ij} with settings P2 or P3, we need to specify an additional element $(k, \ell) \in \mathcal{B}$, as seen in (18) and (19). We shall thus use the notation $\Gamma_{ij}(\mathbf{P}_{k\ell}^2)$ for this purpose.

Figure 12 shows the number of GMRES iterations versus ε_3 , obtained by the proposed method that combines boundary orientation flipping, parameter tuning, and point Jacobi-type preconditioning. The

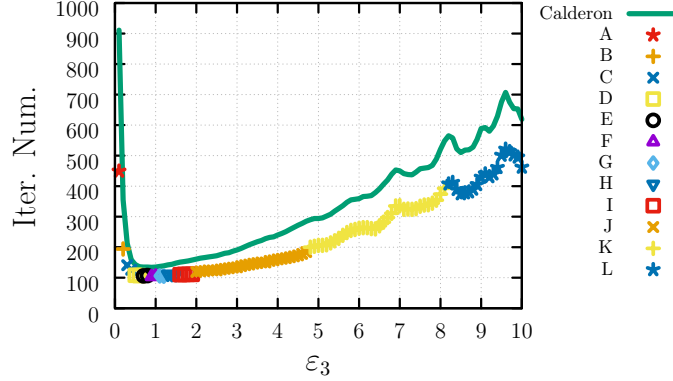


Figure 12: The number of GMRES iterations corresponding to the case in Figure 11.

labels A to L in the figure indicate the specific settings adaptively selected by the proposed method. Each of these configurations is detailed in Table 2. As can be seen, the interface orientations and parameter patterns vary significantly across the different configurations, indicating the necessity of adaptively selecting both in order to optimise convergence. For reference, we also plot the result obtained using the setting fixed as in (24), labelled as Calderon. It is immediately evident that the proposed approach achieves superior performance for all tested cases.

5. Conclusion

This study proposed an extension to the recently developed Calderon-preconditioned BM-BEM [15]. Although the original formulation ensures that the square of the underlying operator has only a few eigenvalue accumulation points with finite absolute values, these eigenvalues may still be widely spread, thereby deteriorating the conditioning of the resulting algebraic system in the BEM.

To address this issue, we first tuned the relevant parameters to cluster the accumulation points as tightly as possible. We then applied a point Jacobi-like preconditioning to further enhance the clustering. Both of these steps are made possible by having analytically identified the eigenvalue accumulation points of the relevant operator in a general setting. The resulting formulation achieves improved efficiency in the BM-BIE for transmission problems involving multiple materials with significantly different material constants.

We plan to extend the present approach to transmission problems in elastodynamics and electromagnetics in 3D. It would also be of interest to apply the proposed BM-BEM to frequency-differentiated Helmholtz' equation for wide-band frequency sweeps [18, 19]. Furthermore, we intend to explore a range of applications, including topology optimisation [20, 21].

Appendix A. Calderon preconditioned BM-BIE for a specific geometry

As an example of the formulation presented in Section 2.2, we here derive the Calderon-preconditioned BIE system corresponding to wave scattering by the composite material shown in Figure A.1.

Table 2: List of interface orientations and BM-type parameter patterns selected by the proposed strategy for each configuration A–L in the scattering problem illustrated in Figure 11.

A	$\Gamma_{23}(\mathbf{P}^1)$	$\Gamma_{24}(\mathbf{P}^1)$	$\Gamma_{34}(\mathbf{P}_{12}^2)$	$\Gamma_{45}(\mathbf{P}_{52}^2)$	$\Gamma_{52}(\mathbf{P}^1)$	$\Gamma_{53}(\mathbf{P}^1)$
B	$\Gamma_{23}(\mathbf{P}^1)$	$\Gamma_{24}(\mathbf{P}^1)$	$\Gamma_{43}(\mathbf{P}_{14}^3)$	$\Gamma_{54}(\mathbf{P}^1)$	$\Gamma_{52}(\mathbf{P}^1)$	$\Gamma_{35}(\mathbf{P}_{12}^2)$
C	$\Gamma_{23}(\mathbf{P}^1)$	$\Gamma_{24}(\mathbf{P}^1)$	$\Gamma_{43}(\mathbf{P}_{23}^2)$	$\Gamma_{54}(\mathbf{P}^1)$	$\Gamma_{52}(\mathbf{P}^1)$	$\Gamma_{35}(\mathbf{P}_{12}^2)$
D	$\Gamma_{32}(\mathbf{P}_{12}^2)$	$\Gamma_{24}(\mathbf{P}^1)$	$\Gamma_{43}(\mathbf{P}^1)$	$\Gamma_{45}(\mathbf{P}^1)$	$\Gamma_{25}(\mathbf{P}^1)$	$\Gamma_{53}(\mathbf{P}_{43}^2)$
E	$\Gamma_{32}(\mathbf{P}_{12}^2)$	$\Gamma_{24}(\mathbf{P}^1)$	$\Gamma_{43}(\mathbf{P}^1)$	$\Gamma_{45}(\mathbf{P}^1)$	$\Gamma_{25}(\mathbf{P}^1)$	$\Gamma_{53}(\mathbf{P}_{15}^3)$
F	$\Gamma_{32}(\mathbf{P}_{12}^2)$	$\Gamma_{42}(\mathbf{P}^1)$	$\Gamma_{43}(\mathbf{P}^1)$	$\Gamma_{45}(\mathbf{P}^1)$	$\Gamma_{25}(\mathbf{P}_{12}^2)$	$\Gamma_{53}(\mathbf{P}_{15}^3)$
G	$\Gamma_{32}(\mathbf{P}_{12}^2)$	$\Gamma_{42}(\mathbf{P}^1)$	$\Gamma_{43}(\mathbf{P}^1)$	$\Gamma_{45}(\mathbf{P}^1)$	$\Gamma_{25}(\mathbf{P}_{12}^2)$	$\Gamma_{53}(\mathbf{P}_{45}^3)$
H	$\Gamma_{23}(\mathbf{P}^1)$	$\Gamma_{42}(\mathbf{P}_{12}^2)$	$\Gamma_{34}(\mathbf{P}^1)$	$\Gamma_{54}(\mathbf{P}_{15}^3)$	$\Gamma_{25}(\mathbf{P}^1)$	$\Gamma_{35}(\mathbf{P}^1)$
I	$\Gamma_{23}(\mathbf{P}^1)$	$\Gamma_{42}(\mathbf{P}_{12}^2)$	$\Gamma_{34}(\mathbf{P}^1)$	$\Gamma_{54}(\mathbf{P}_{34}^2)$	$\Gamma_{25}(\mathbf{P}^1)$	$\Gamma_{35}(\mathbf{P}^1)$
J	$\Gamma_{23}(\mathbf{P}^1)$	$\Gamma_{24}(\mathbf{P}^1)$	$\Gamma_{34}(\mathbf{P}_{24}^2)$	$\Gamma_{45}(\mathbf{P}_{12}^2)$	$\Gamma_{52}(\mathbf{P}^1)$	$\Gamma_{53}(\mathbf{P}^1)$
K	$\Gamma_{23}(\mathbf{P}^1)$	$\Gamma_{24}(\mathbf{P}^1)$	$\Gamma_{43}(\mathbf{P}_{12}^2)$	$\Gamma_{54}(\mathbf{P}_{24}^2)$	$\Gamma_{25}(\mathbf{P}^1)$	$\Gamma_{35}(\mathbf{P}_{12}^2)$
L	$\Gamma_{23}(\mathbf{P}^1)$	$\Gamma_{24}(\mathbf{P}^1)$	$\Gamma_{43}(\mathbf{P}_{12}^2)$	$\Gamma_{54}(\mathbf{P}_{14}^2)$	$\Gamma_{25}(\mathbf{P}^1)$	$\Gamma_{35}(\mathbf{P}_{12}^2)$

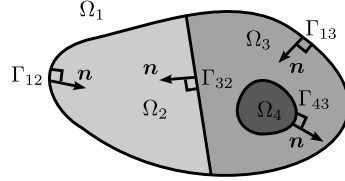


Figure A.1: Composite material with 4 subdomains. The normal direction on $\Gamma_{ij} := \partial\Omega_i \cap \partial\Omega_j$ is defined to point outward from Ω_i .

Let us first consider, for example, the index set \mathcal{T}_3 . We have $\mathcal{T}_3 = \{1, 2, 4\}$, since Ω_3 shares boundaries with Ω_1 , Ω_2 , and Ω_4 . The subsets $\mathcal{T}_3^+ = \{2\}$ and $\mathcal{T}_3^- = \{1, 4\}$ follow from the orientation of the normal vectors: the normal on Γ_{32} is defined to point outward from Ω_3 , whereas those on Γ_{13} and Γ_{43} point inward to Ω_3 . We then collect all index pairs (i, j) such that Γ_{ij} exists into an ordered set, denoted by $\mathcal{B} = \{(1, 2), (1, 3), (3, 2), (4, 3)\}$. The ordering of the pairs can be chosen arbitrarily, but must remain fixed once specified. In accordance with the order specified by \mathcal{B} , the traces u_{ij} and w_{ij} are collected into the sequences $u_{\mathcal{B}} = (u_{12}, u_{13}, u_{32}, u_{43})^t$ and $w_{\mathcal{B}} = (w_{12}, w_{13}, w_{32}, w_{43})^t$, respectively. The BIEs (5), derived as the trace of the integral representation in Ω_j to Γ_{ij} , are then listed in the order specified by \mathcal{B} as follows:

$$-\alpha_1 \left(\frac{\mathcal{I}}{2} - \mathcal{D}_{12}^2 \right) u_{12} + \alpha_1 \mathcal{D}_{32}^2 u_{32} - \alpha_1 \varepsilon_2 \mathcal{S}_{12}^2 w_{12} - \alpha_1 \varepsilon_2 \mathcal{S}_{32}^2 u_{32} = 0, \quad (\text{A.1})$$

$$-\alpha_1 \left(\frac{\mathcal{I}}{2} - \mathcal{D}_{13}^3 \right) u_{13} - \alpha_1 \mathcal{D}_{32}^3 u_{32} + \alpha_1 \mathcal{D}_{43}^3 u_{43} - \alpha_1 \varepsilon_3 \mathcal{S}_{13}^3 w_{13} + \alpha_1 \varepsilon_3 \mathcal{S}_{32}^3 w_{32} - \alpha_1 \varepsilon_3 \mathcal{S}_{43}^3 w_{43} = 0, \quad (\text{A.2})$$

$$\alpha_1 \mathcal{D}_{12}^2 u_{12} - \alpha_1 \left(\frac{\mathcal{I}}{2} - \mathcal{D}_{32}^2 \right) u_{32} - \alpha_1 \varepsilon_2 \mathcal{S}_{12}^2 w_{12} - \alpha_1 \varepsilon_2 \mathcal{S}_{32}^2 w_{32} = 0, \quad (\text{A.3})$$

$$\alpha_1 \mathcal{D}_{13}^3 u_{13} - \alpha_1 \mathcal{D}_{32}^3 u_{32} - \alpha_1 \left(\frac{\mathcal{I}}{2} - \mathcal{D}_{43}^3 \right) u_{43} - \alpha_1 \varepsilon_3 \mathcal{S}_{13}^3 w_{13} + \alpha_1 \varepsilon_3 \mathcal{S}_{32}^3 w_{32} - \alpha_1 \varepsilon_3 \mathcal{S}_{43}^3 w_{43} = 0, \quad (\text{A.4})$$

in which all the equations are multiplied by the same constant $-\alpha_1$. Subsequently, the BIEs (6) are listed, again in accordance with the order \mathcal{B} as

$$\left(\frac{\mathcal{I}}{2} + \mathcal{W}_{12}^1\right) u_{12} + \mathcal{W}_{13}^1 u_{13} + \varepsilon_1 \left(\frac{\alpha_1 \mathcal{I}}{2} - \mathcal{V}_{12}^1\right) w_{12} - \varepsilon_1 \mathcal{V}_{13}^1 w_{13} = 0, \quad (\text{A.5})$$

$$\mathcal{W}_{12}^1 u_{12} + \left(\frac{\mathcal{I}}{2} + \mathcal{W}_{13}^1\right) u_{13} - \varepsilon_1 \mathcal{V}_{12}^1 w_{12} + \varepsilon_1 \left(\frac{\alpha_1 \mathcal{I}}{2} - \mathcal{V}_{13}^1\right) w_{13} = 0, \quad (\text{A.6})$$

$$-\mathcal{W}_{13}^3 u_{13} + \left(\frac{\mathcal{I}}{2} + \mathcal{W}_{32}^3\right) u_{32} - \mathcal{W}_{43}^3 u_{43} + \varepsilon_3 \mathcal{V}_{13}^3 w_{13} + \varepsilon_3 \left(\frac{\alpha_3 \mathcal{I}}{2} - \mathcal{V}_{32}^3\right) w_{32} + \varepsilon_3 \mathcal{V}_{43}^3 w_{43} = 0, \quad (\text{A.7})$$

$$\left(\frac{\mathcal{I}}{2} + \mathcal{W}_{43}^4\right) u_{43} + \varepsilon_4 \left(\frac{\alpha_4 \mathcal{I}}{2} - \mathcal{V}_{43}^4\right) w_{43} = 0, \quad (\text{A.8})$$

where the BM operators $\mathcal{V}_{jk}^i := \mathcal{S}_{jk}^i + \alpha_i (\mathcal{D}_{jk}^i)^*$ and $\mathcal{W}_{jk}^i := \mathcal{D}_{jk}^i + \alpha_i \mathcal{N}_{jk}^i$ are defined. Then, all the BIEs (A.1)–(A.8) are assembled in the specified order to form the whole system (12).

Appendix B. Eigenvalue distribution of \mathcal{A}^2

Here, we examine the eigenvalue distribution of the square of the coefficient matrix obtained by discretising the operator \mathcal{A} in (12) using a collocation method with constant elements. Figure B.1 shows the distributions for the configurations in Figures 3 (with 3600 boundary elements) and 6 (1800 elements). For both cases, the angular frequency and material parameters are set to $\omega = 1$, $\varepsilon_1 = 1$, $\varepsilon_2 = 2$, and $\varepsilon_3 = 3$. In the figure, the accumulation points of the eigenvalues of the operator \mathcal{A}^2 are also plotted. These can be

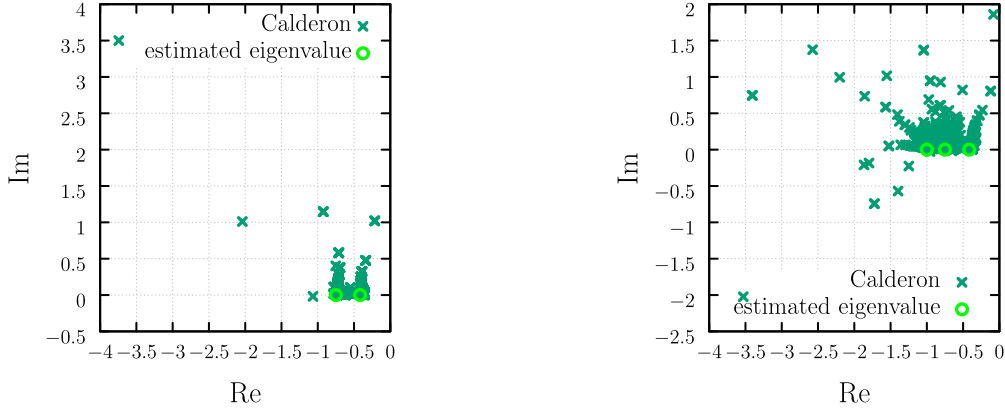


Figure B.1: Eigenvalue distribution of the Calderon-preconditioned \mathcal{A}^2 for the configuration in Figure 3 (left) and that in Figure 6 (right). Theoretically derived clustering points of the operator \mathcal{A}^2 from (15) are also plotted.

evaluated using (15) as $\frac{\alpha_1(1+\varepsilon_2)}{4} = -0.75$ and $\frac{\alpha_1(1+\varepsilon_2/\varepsilon_3)}{4} \approx -0.417$ for the case of the concentric spheres corresponding to Figure 3, and $\frac{\alpha_1(1+\varepsilon_2)}{4} = -0.75$, $\frac{\alpha_1(1+\varepsilon_3)}{4} = -1$, and $\frac{\alpha_1(1+\varepsilon_2/\varepsilon_3)}{4} \approx -0.417$ for Figure 6. As observed, the eigenvalues of the coefficient matrix cluster around the predicted points, leading to faster convergence of GMRES.

Acknowledgements. The point Jacobi-type preconditioning used in this paper benefited greatly from discussions with Dr Yasuhiro Matsumoto of the Institute of Science Tokyo. The authors also acknowledge that this work was supported by JSPS KAKENHI Grant Number 21K19764. This work is also partially supported by “Joint Usage/Research Center for Interdisciplinary Large-scale Information Infrastructures (JHPCN)” in Japan (Project ID: jh240031 and jh250045).

References

- [1] I. Akduman, R. Kress, Direct and inverse scattering problems for inhomogeneous impedance cylinders of arbitrary shape, *Radio Science* 38 (3), iISBN: 0048-6604 Publisher: Wiley Online Library (2003).
- [2] M. Hammer, D. Schweitzer, B. Michel, E. Thamm, A. Kolb, Single scattering by red blood cells, *Applied Optics* 37 (31) (1998) 7410–7418, publisher: OSA.
- [3] W. C. Chew, E. Michielssen, J. Song, J.-M. Jin, Fast and efficient algorithms in computational electromagnetics, Artech House, Inc., 2001.
- [4] C. Müller, Foundations of the mathematical theory of electromagnetic waves, Vol. 155, Springer Science & Business Media, 2013.
- [5] R. Kleinman, P. Martin, On single integral equations for the transmission problem of acoustics, *SIAM Journal on Applied Mathematics* 48 (2) (1988) 307–325, publisher: SIAM.
- [6] M. Costabel, E. Stephan, A direct boundary integral equation method for transmission problems, *Journal of mathematical analysis and applications* 106 (2) (1985) 367–413.
- [7] S. H. Christiansen, J.-C. Nédélec, Des préconditionneurs pour la résolution numérique des équations intégrales de frontière de l’acoustique, *Comptes Rendus de l’Académie des Sciences-Series I-Mathematics* 330 (7) (2000) 617–622.
- [8] X. Antoine, Y. Boubendir, An integral preconditioner for solving the two-dimensional scattering transmission problem using integral equations, *International Journal of Computer Mathematics* 85 (10) (2008) 1473–1490, publisher: Taylor & Francis.
- [9] K. Niino, N. Nishimura, Preconditioning based on Calderon’s formulae for periodic fast multipole methods for Helmholtz’equation, *Journal of Computational Physics* 231 (1) (2012) 66–81, publisher: Elsevier.
- [10] Y. Saad, M. H. Schultz, GMRES: A generalized minimal residual algorithm for solving nonsymmetric linear systems, *SIAM Journal on scientific and statistical computing* 7 (3) (1986) 856–869, publisher: SIAM.
- [11] R. Misawa, K. Niino, N. Nishimura, Boundary integral equations for calculating complex eigenvalues of transmission problems, *SIAM Journal on Applied Mathematics* 77 (2) (2017) 770–788, publisher: SIAM.
- [12] X. Claeys, R. Hiptmair, E. Spindler, A second-kind galerkin boundary element method for scattering at composite objects, *BIT Numerical Mathematics* 55 (2015) 33–57.
- [13] R. Hiptmair, C. Jerez-Hanckes, Multiple traces boundary integral formulation for Helmholtz transmission problems, *Advances in Computational Mathematics* 37 (1) (2012) 39–91, publisher: Springer.
- [14] A. Burton, G. Miller, The application of integral equation methods to the numerical solution of some exterior boundary-value problems, *Proceedings of the Royal Society of London. A. Mathematical and Physical Sciences* 323 (1553) (1971) 201–210, publisher: The Royal Society London.
- [15] Y. Matsumoto, A. Yoshiki, H. Isakari, Calderon-preconditioned boundary integral equations of the Burton-Miller type for transmission problems, *arXiv preprint arXiv:2312.12787* (2023).
- [16] C.-J. Zheng, H.-B. Chen, H.-F. Gao, L. Du, Is the Burton–Miller formulation really free of fictitious eigenfrequencies?, *Engineering Analysis with Boundary Elements* 59 (2015) 43–51, publisher: Elsevier.
- [17] K. Tomoyasu, H. Kotani, H. Isakari, Calderon-preconditioned BEMs for frequency-differentiated boundary-value problems of Helmholtz’ equation, *Transactions of Japan Society for Computational Methods in Engineering* 24 (2024) 43–53.
- [18] L. Chen, H. Lian, Y. Xu, S. Li, Z. Liu, E. Atroshchenko, P. Kerfriden, Generalized isogeometric boundary element method for uncertainty analysis of time-harmonic wave propagation in infinite domains, *Applied Mathematical Modelling* 114 (2023) 360–378.
- [19] J. Kook, J. S. Jensen, S. Wang, Acoustical topology optimization of zwicker’s loudness with padé approximation, *Computer Methods in Applied Mechanics and Engineering* 255 (2013) 40–66.
- [20] K. Nakamoto, H. Isakari, T. Takahashi, T. Matsumoto, A fast topology optimisation for material-and geometry-independent cloaking devices with the BEM and the \mathcal{H} -matrix method, *arXiv preprint arXiv:1611.08072* (2016).
- [21] H. Isakari, K. Kuriyama, S. Harada, T. Yamada, T. Takahashi, T. Matsumoto, A topology optimisation for three-dimensional acoustics with the level set method and the fast multipole boundary element method, *Mechanical Engineering Journal* 1 (4) (2014) CM0039–CM0039, publisher: The Japan Society of Mechanical Engineers.